Applied Mathematics and Computation 217 (2010) 2084–2096

Contents lists available at ScienceDirect

Applied Mathematics and Computation

journal homepage: www.elsevier.com/locate/amc

Theoretical analysis of high speed spindle air bearings by a hybrid numerical method

Cheng-Chi Wang [a,*], Her-Terng Yau [b]

[a] Department of Mechanical Engineering, Far East University, Hsin-Shih, Tainan, Taiwan
[b] Department of Electrical Engineering, National Chin-Yi University of Technology, Taichung, Taiwan

ARTICLE INFO

Keywords:
High speed spindle air bearing
Hybrid numerical method
Differential transformation method
Quasi-periodic

ABSTRACT

To study the behavior of the high speed spindle air bearing (HSSAB) system, we conduct the research by means of a hybrid numerical method which combines the differential transformation method and the finite difference method in this paper. According to the results of the research, the flexible rotor center is found to include a complex dynamic behavior that comprises periodic, sub-harmonic and quasi-periodic responses. In addition, as the rotor mass and the bearing number are increased, there will be some changes taking place in the dynamic behavior of the bearing system. The results are proven to have no conflict with those of the other numerical methods, which enables an effective means in gaining insights into the nonlinear dynamics of HSSAB systems.

1. Introduction

Aerodynamic bearings are characterized by low noise under rotation and by their low frictional losses. As a result, they are frequently employed within precision instruments, where they yield zero friction when the instruments are used as null devices, and within high-speed electrical motors. In 1963, Ausman [1] solved the linearized Reynolds equation of self-acting bearings to investigate the stability of the static equilibrium position of the shaft. Botman [2] observed non-synchronous vibrations at speeds in excess of twice the system critical speed on a high-speed rigid rotor-damper system. Nikolajsen and Holmes [3] observed non-synchronous vibrations in a flexible, symmetric rotor on two identical plain journal bearings supported by centralized squeeze film dampers. Li and Taylor [4] also observed sub-harmonic motion in rotor-bearing systems, and at around the same time, Ehrich [5] published his observations of 8th and 9th sub-harmonic vibration in a turbomachine.

In 1985, Gero and Ettles [6] evaluated the relative precision of the FDM and FEM approaches when applied to a steady, isoviscous, incompressible lubrication problem. In their study, it was assumed that the solution of a complicated coupled problem could be derived by solving a sequential series of simple, uncoupled, steady problems. The results for two-dimensional bearings demonstrated that the relative errors of the FDM solutions were smaller than those associated with the FEM approach. Furthermore, it was shown that the FDM approach was more rapid than the FEM technique, with an average CPU time of 0.15 s as compared to 0.17 s for the FEM method.

In 1994, Malik and Bert [7] considered the Differential Quadrature Method (DQM), and applied it for the first time to the solution of steady state oil and air lubrication problems in self-acting hydrodynamic bearings. The quadrature solutions of the Reynolds equation for the case of incompressible lubrication were compared with the exact solutions of finite-length bearings. Furthermore, the quadrature solutions of the compressible Reynolds equation for finite-length plain journal bear-

* Corresponding author.
E-mail addresses: wccpipn@yahoo.com.tw, ccwang@cc.feu.edu.tw (C.-C. Wang), pan1012@ms52.hinet.net (H.-T. Yau).

0096-3003/$ - see front matter © 2010 Elsevier Inc. All rights reserved.
doi:10.1016/j.amc.2010.07.008

ings were compared with those obtained using the FED and FEM approaches. From 2007 to 2009, Wang and co-workers [8–11] provide a series of further understanding of gas film rotor-bearing systems and show the dynamic behavior of system with respect to rotor mass and bearing number.

The remainder of this study is organized as follows. Section 2 develops a mathematical model describing the time-dependent motions of the rotor center of HSSAB. Due to the nonlinearity of the air film pressure in this bearing system, determining the Reynolds equation solutions is very difficult. Accordingly, Sections 2.2 and 2.3 develop a hybrid method combining the finite difference method (FDM) and the differential transformation method (DTM) to obtain the required solutions. The solutions are then compared with those obtained using the SOR (Successive Over Relation) method. Section 3 presents the simulation results obtained using the proposed hybrid method for the vibrations of the rotor center for various rotor masses. Finally, Section 4 draws some brief conclusions.

2. Mathematical modeling

2.1. Modified Reynolds equation and rotor dynamics

The aerostatic bearings model incorporates the following design assumptions:

(a) Air lubricating films are very nearly isothermal because the ability of the bearing materials to conduct away heat is greater than the heat generating capacity of the air film. Thus, the flow is assumed isothermal.
(b) As gas viscosity is somewhat insensitive to changes in pressure, and the temperature is virtually constant, we may assume the gas viscosity to be constant.
(c) The mass flow inside and outside of the gas bearing element is equal to the mass flow into the orifice.
(d) The flow of gas in and out of the sides of the bearing (side flow) is neglected.

The pressure distribution in the gas film between the shaft and the bushing is modeled by the Reynolds equation as follows:

$$\frac{\partial}{\partial \bar{x}}\left(\bar{p}\bar{h}^3\frac{\partial \bar{p}}{\partial \bar{x}}\right)+\frac{\partial}{\partial \bar{y}}\left(\bar{p}\bar{h}^3\frac{\partial \bar{p}}{\partial \bar{y}}\right)+12\eta\rho\frac{p_a}{\rho_a}\tilde{v}=12\eta\frac{\partial(\bar{p}\bar{h})}{\partial t}+6\eta u_1\frac{\partial}{\partial \bar{x}}(\bar{p}\bar{h})+6\eta w_1\frac{\partial}{\partial \bar{y}}(\bar{p}\bar{h}). \tag{1}$$

The dimensionless form of the Reynolds equation is given by:

$$\frac{\partial}{\partial X}\left(PH^3\frac{\partial P}{\partial X}\right)+\frac{\partial}{\partial Y}\left(PH^3\frac{\partial P}{\partial Y}\right)+\tilde{Q}\delta_i=\Lambda_t\frac{\partial}{\partial \tau}(PH)+\Lambda_x\frac{\partial}{\partial X}(PH)+\Lambda_y\frac{\partial}{\partial Y}(PH), \tag{2}$$

where Λ_x and Λ_y are the bearing numbers in the x- and y-directions, respectively, and Λ_t is bearing number corresponding with rotational speed of rotor. $\tilde{Q}$ is the mass flow factor of the orifice. It is noted that $\delta_i = 1$ at the orifice entrance, and that $\delta_i = 0$ at the orifice exit.

The following dimensionless parameters are defined:

$$X=\frac{\bar{x}}{L},\quad Y=\frac{\bar{y}}{L},\quad H=\frac{\bar{h}}{h_m},\quad P=\frac{\bar{p}}{p_0},\quad \Lambda_t=\frac{12\eta\omega L^2}{h_m^2 p_o},\quad \Lambda_x=\frac{6\eta u_1 L}{h_m^2 p_o},\quad \Lambda_y=\frac{6\eta w_1 L}{h_m^2 p_o},\quad \tilde{Q}=\frac{12\eta L^2 p_a}{h_m^3 p_0^2\rho_a}\rho\tilde{v}.$$

Adopting the assumptions of an adiabatic process and a non-viscous flow, it can be shown that the mass flow rate is given by:

$$\dot{m}=Ap_0\phi\sqrt{\frac{2\rho_0}{p_0}}\varphi, \tag{3}$$

$$\varphi=\begin{cases}\left[\frac{k}{2}\left(\frac{2}{k+1}\right)^{(k+1)/(k-1)}\right]^{1/2}, & \frac{\bar{p}}{p_0}\leqslant\beta_k,\\ \left\{\frac{k}{k-1}\left[\left(\frac{\bar{p}}{p_0}\right)^{2/k}-\left(\frac{\bar{p}}{p_0}\right)^{(k+1)/k}\right]\right\}^{1/2}, & \frac{\bar{p}}{p_0}>\beta_k,\end{cases} \tag{4}$$

where A is the cross-sectional area of the orifice, k is the ratio of the specific heat, p_0 is the supplied pressure, ϕ is the coefficient of the mass flow rate through the orifice, and $\beta_k=\frac{p_c}{p_0}=\left(\frac{2}{k+1}\right)^{k/(k-1)}$.

Fig. 1 presents the gas journal bearing configuration considered in the present study. It is observed that two sets of eight orifices are arranged evenly around the circumference of the bearing at quarter-station positions.

The boundary conditions are shown as follows:

1. The atmosphere boundary condition: $P=\frac{p_a}{p_0}$.
2. The periodic boundary condition: $P(Z) = P(Z + 2\pi)$.
3. The symmetric boundary condition: $\frac{\partial P}{\partial X}=0$.

In the transient state, the equations of motion of rotor center (X,Y) can be written in Cartesian coordinate form as

$$m_r \frac{d^2X}{dt^2} + K_p(X - X^*) = m_r \rho\omega^2 \cos\omega t, \tag{5}$$

$$m_r \frac{d^2Y}{dt^2} + K_p(Y - Y^*) = m_r \rho\omega^2 \cos\omega t, \tag{6}$$

where (X^*,Y^*) is journal center, ρ is the mass eccentricity of the rotor, K_P is the stiffness of the shaft, and ω is the rotational speed of the shaft. The resultant forces acting on the journal center in the horizontal and vertical directions are balancing forces. They can be shown that the forces applied to journal center are given by

$$F^*_{gfx} = K_p(X - X^*)/2, \tag{7}$$

$$F^*_{gfy} = K_p(Y - Y^*)/2. \tag{8}$$

Computing the motions of the rotor center and journal center is an iterative procedure which first determines the acceleration, then the velocity, and finally the displacement, step-by-step over time. The computation procedure begins by specifying an initial static equilibrium state. The initial displacement of the rotor (X_o,Y_o) corresponds to the static equilibrium position and defines the gap H between the shaft and the journal bearing. The initial velocity of the rotor is assumed to be zero.

2.2. Hybrid method integrating SOR method and finite difference method (SOR&FDM)

In solving the Reynolds' equation, Eq. (2) is discretized using the central-difference scheme in the x- and y-directions and the implicit-back-difference scheme in time τ. For simplicity, a uniform mesh size is used. If Eq. (2) is to be solved directly, there will be five unknowns. Accordingly, the SOR (Successive Over Relation) method [8] is employed in the present computations since its use reduces the number of unknowns from five to three. The pressure distribution at each time step is obtained using an iterative calculation process. Thus, there will be three unknowns (I, $I-1$, and $I+1$) in the x-direction at each incremental time interval. The other two unknowns ($J+1$ and $J-1$) in the y-direction are substituted for the last iterative values. Finally, all of the equations are substituted into a tri-diagonal matrix and solved using a process of Gauss elimination.

2.3. Hybrid method integrating differential transformation method and finite difference method (DTM&FDM)

Differential transformation is one of the most widely used techniques for solving differential equations due to its rapid convergence rate and minimal calculation error. A further advantage of this method over the integral transformation approach is its ability to solve nonlinear differential equations.

In solving the Reynolds equation for the current micro gas bearing system, the differential transformation method is used for taking transformation with respect to the time domain τ, and hence Eq. (2) becomes

$$\begin{aligned}&\frac{\partial P}{\partial X}\otimes J\otimes\frac{\partial P}{\partial X} + P\otimes\frac{\partial J}{\partial X}\otimes\frac{\partial P}{\partial X} + P\otimes J\otimes\frac{\partial^2 P}{\partial X^2} + \frac{\partial P}{\partial Y}\otimes J\otimes\frac{\partial P}{\partial Y} + P\otimes\frac{\partial J}{\partial Y}\otimes\frac{\partial P}{\partial Y} + P\otimes J\otimes\frac{\partial^2 P}{\partial Y^2} + \widetilde{Q}\,\delta_i\\ &\quad = \Lambda_t\frac{\partial P}{\partial\tau}\otimes H + \Lambda_t\frac{\partial H}{\partial\tau}\otimes P + \Lambda_x\frac{\partial P}{\partial X}\otimes H + \Lambda_x\frac{\partial H}{\partial X}\otimes P + \Lambda_y\frac{\partial P}{\partial Y}\otimes H + \Lambda_y\frac{\partial H}{\partial Y}\otimes P,\end{aligned} \tag{9}$$

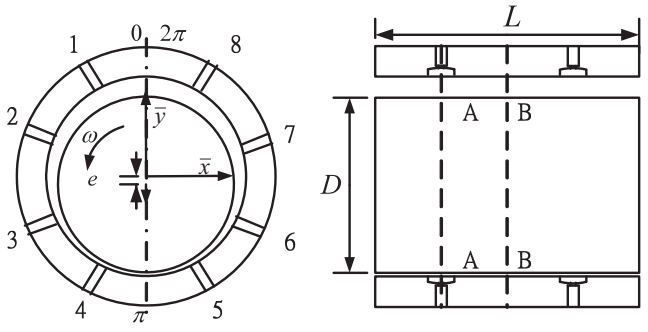

Fig. 1. Journal bearing configuration.

where

$$J(k) = H^3 = H \otimes H \otimes H = \sum_{l=0}^{k} H_{i,j}(k-l) \sum_{m=0}^{l} H_{i,j}(l-m) H_{i,j}(m) \tag{10}$$

and "$\otimes$" denotes the convolution operation in the K domain. If $z(t) = f(t)g(t)$, $f(t) = D^{-1}[F(k)]$, and $g(t) = D^{-1}[G(k)]$, then $D[z(t)] = D[f(t)g(t)] = F(k) \otimes G(k) = \sum_{l=0}^{k} F(l)G(k-l) = \sum_{l=0}^{k} F(k-l)G(l)$ [10,11].

The finite difference method is then used to discretize Eq. (9) with respect to the x- and y-directions. Note that Eq. (9) is discretized using the second-order accurate central-difference scheme for both the first and the second derivatives.

Substituting Eq. (10) into Eq. (9) yields

$$\begin{aligned}
&\sum_{l=0}^{k} \left(\frac{P_{i+1,j}(k-l) - P_{i-1,j}(k-l)}{2\Delta X} \right) \sum_{m=0}^{l} \left[J_{i,j}(l-m) \left(\frac{Q_{i+1,j}(m) - Q_{i-1,j}(m)}{2\Delta X} \right) \right] \\
&\quad + \sum_{l=0}^{k} P_{i,j}(k-l) \sum_{m=0}^{l} \left[\left(\frac{J_{i+1,j}(l-m) - J_{i-1,j}(l-m)}{2\Delta X} \right) \cdot \left(\frac{P_{i+1,j}(m) - P_{i-1,j}(m)}{2X} \right) \right] \\
&\quad + \sum_{l=0}^{k} P_{i,j}(k-l) \sum_{m=0}^{l} \left[J_{i,j}(l-m) \cdot \left(\frac{P_{i+1,j}(m) - 2P_{i,j}(m) + P_{i-1,j}(m)}{(\Delta X)^2} \right) \right] \\
&\quad + \sum_{l=0}^{k} \left(\frac{P_{i,j+1}(k-l) - P_{i,j-1}(k-l)}{2\Delta Y} \right) \sum_{m=0}^{l} \left[J_{i,j}(l-m) \left(\frac{Q_{i,j+1}(m) - Q_{i,j-1}(m)}{2\Delta Y} \right) \right] \\
&\quad + \sum_{l=0}^{k} P_{i,j}(k-l) \sum_{m=0}^{l} \left[\left(\frac{J_{i,j+1}(l-m) - J_{i,j-1}(l-m)}{2\Delta Y} \right) \cdot \left(\frac{P_{i,j+1}(m) - P_{i,j-1}(m)}{2\Delta Y} \right) \right] \\
&\quad + \sum_{l=0}^{k} P_{i,j}(k-l) \sum_{m=0}^{l} \left[J_{i,j}(l-m) \cdot \left(\frac{P_{i,j+1}(m) - 2P_{i,j}(m) + P_{i,j-1}(m)}{(\Delta Y)^2} \right) \right] + \widetilde{Q}\,\delta_i \\
&= \Lambda_t \cdot \sum_{l=0}^{k} \left[\left(\frac{l+1}{\widetilde{H}} \right) P_{i,j}(k-l) \cdot H_{i,j}(l+1) \right] + \Lambda_t \cdot \sum_{l=0}^{k} \left[\left(\frac{l+1}{\widetilde{H}} \right) H_{i,j}(k-l) \cdot P_{i,j}(l+1) \right] \\
&\quad + \Lambda_x \cdot \sum_{l=0}^{k} \left[\left(\frac{P_{i+1,j}(k-l) - P_{i-1,j}(k-l)}{2\Delta Y} \right) \cdot H_{i,j}(l) \right] + \Lambda_x \cdot \sum_{l=0}^{k} \left[\left(\frac{H_{i+1,j}(k-l) - H_{i-1,j}(k-l)}{2\Delta X} \right) \cdot P_{i,j}(l) \right] \\
&\quad + \Lambda_y \cdot \sum_{l=0}^{k} \left[\left(\frac{P_{i,j+1}(k-l) - P_{ij-1}(k-l)}{2\Delta Y} \right) \cdot H_{i,j}(l) \right] + \Lambda_y \cdot \sum_{l=0}^{k} \left[\left(\frac{H_{i,j+1}(k-l) - H_{i,j-1}(k-l)}{2\Delta Y} \right) \cdot P_{i,j}(l) \right].
\end{aligned} \tag{11}$$

From Eq. (11), $P_{i,j}(k)$ is obtained for each time interval, where i and j indicate the node position and k indicates the kth term.

Computing the motions of the rotor center is an iterative procedure which first determines the acceleration, then the velocity, and finally the displacement, step-by-step over time. The computation procedure begins by specifying an initial static equilibrium state. The initial displacement of the rotor (X_o, Y_o) corresponds to the static equilibrium position and defines the gap $H_{i,j}(k)$ between the shaft and the journal bearing. The initial velocity of the rotor is assumed to be zero.

The iterative computation procedure can be summarized as follows:

Step 1: Following a time increment $\Delta\tau$, the new values of the rotor acceleration, velocity, and displacement are calculated to obtain.

Table 1
Comparison of numerical results of rotor center orbits calculated by SOR&FDM and DTM&FDM methods, respectively (for T-periodic motion).

Conditions		Displacement			
		X (nT)		Y (nT)	
		Time step = 0.001	Time step = 0.01	Time step = 0.001	Time step = 0.01
SOR&FDM	m_r = 1.3 kg	−0.3315343711	−0.3315131879	−0.6217047214	−0.621754232
DTM&FDM	Λ_t = 1.27	−0.3315562023	−0.3315321144	−0.6217134332	−0.621732771
SOR&FDM	m_r = 3.46 kg	−0.2681450512	−0.2681524783	−0.261236245	−0.267044675
DTM&FDM	Λ_t = 1.27	−0.2681911341	−0.2681010143	−0.268101956	−0.268140132
SOR&FDM	Λ_t = 2.38	0.2618134124	0.2619497941	0.7031651104	0.7032671983
DTM&FDM	m_r = 2.5 kg	0.2621720747	0.2621772397	0.7037471446	0.7037436364
SOR&FDM	Λ_t = 3.52	−0.51201081123	−0.51831609801	0.25021083144	0.25195381540
DTM&FDM	m_r = 2.5 kg	−0.51187525198	−0.51184543216	0.25081519298	0.25084166217

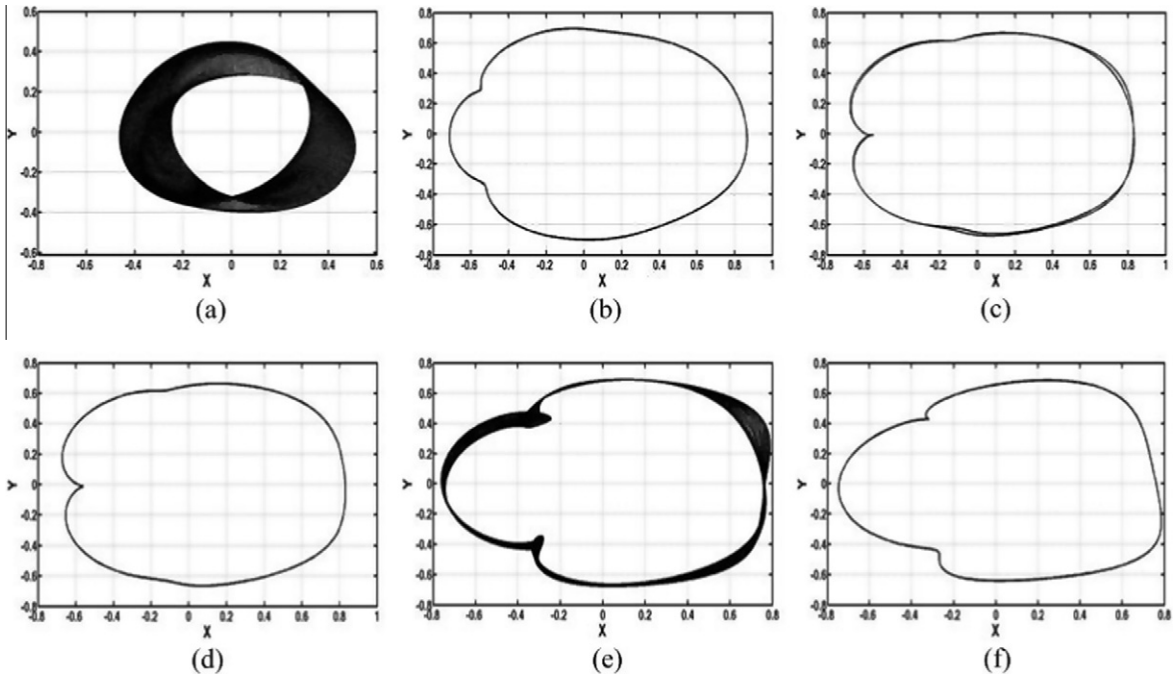

Fig. 2. Dynamic orbits of rotor center at m_r = 1.1, 1.3, 1.9, 1.93, 3.16 and 3.46 kg.

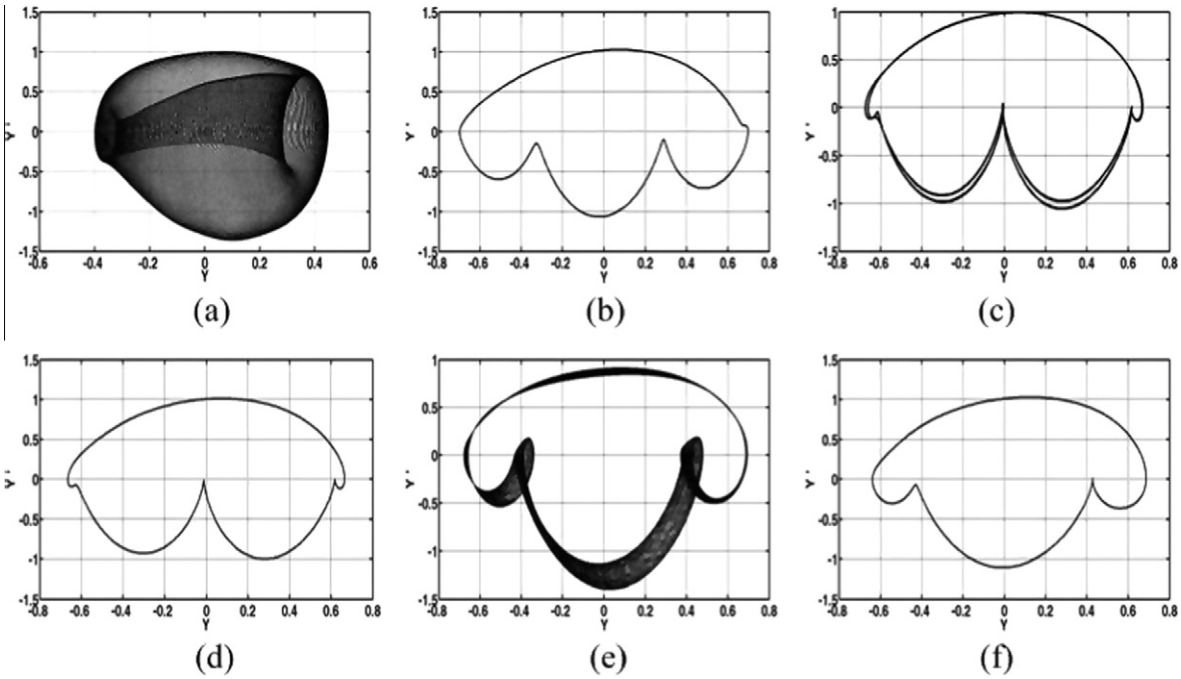

Fig. 3. Phase trajectories of rotor center at m_r = 1.1, 1.3, 1.9, 1.93, 3.16 and 3.46 kg.

Step 2: The displacements of the rotor center obtained from Step 1 can then be determined and the corresponding change in the value of the gap (H) can be calculated. Substituting the new value of H into Eq. (10) gives the new pressure distribution in the gap between the shaft and the journal.

Step 3: The pressure distribution obtained from Step 2 is integrated to estimate the internal force.

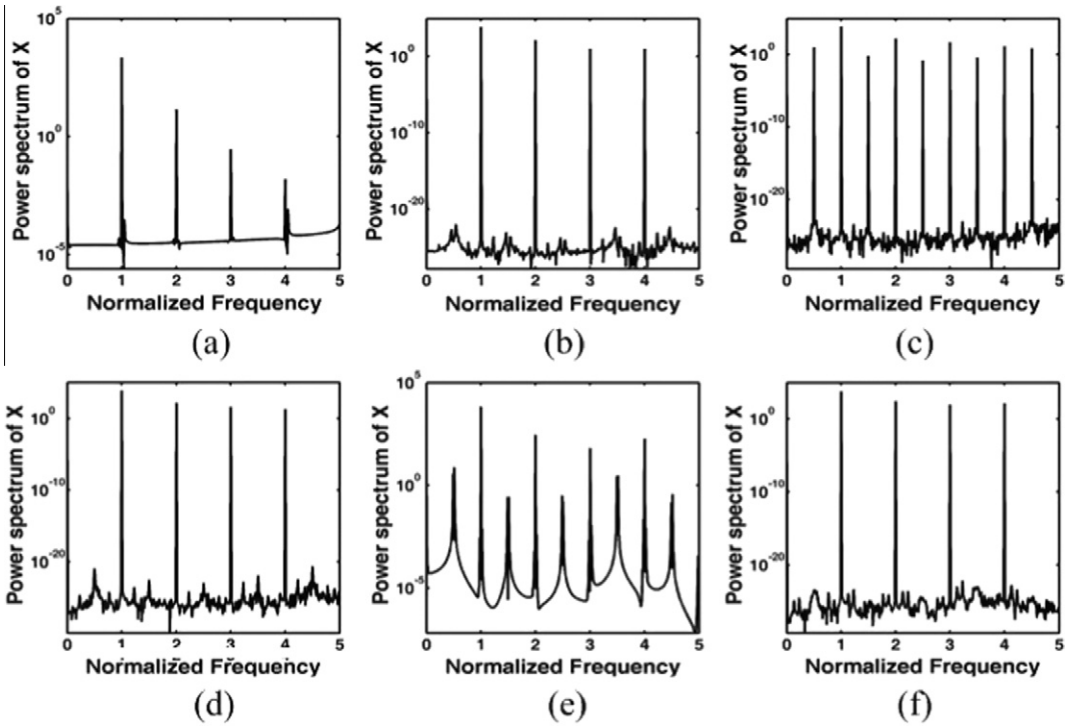

Fig. 4. Power spectra of rotor displacement in horizontal direction at m_r = 1.1, 1.3, 1.9, 1.93, 3.16 and 3.46 kg.

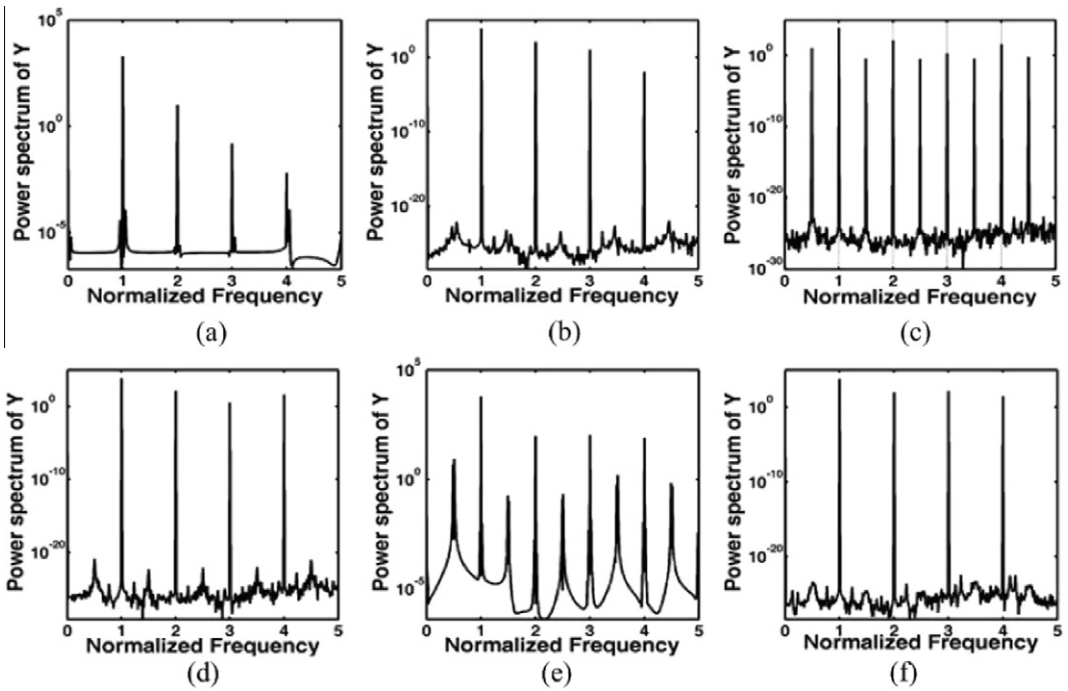

Fig. 5. Power spectra of rotor displacement in vertical direction at m_r = 1.1, 1.3, 1.9, 1.93, 3.16 and 3.46 kg.

Step 4: The displacement and velocity values computed in Step 1, the pressure distribution calculated in Step 2, and the internal force obtained in Step 3 are taken as the new initial conditions. Using this new set of conditions, the calculation procedure returns to Step 1 to compute the changes in the micro gas bearing system during the time interval $\Delta\tau \rightarrow 2\Delta\tau$.

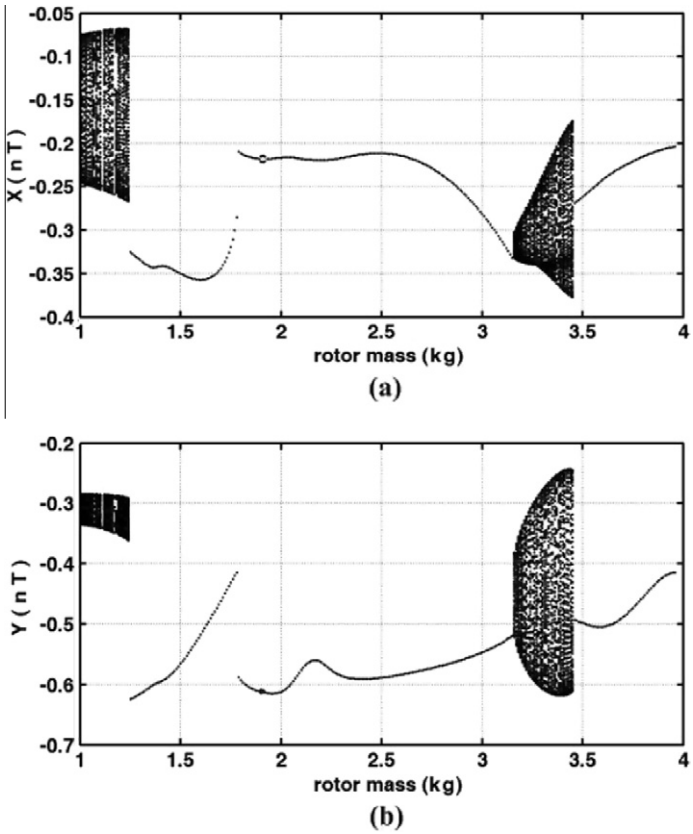

Fig. 6. Bifurcation diagrams versus rotor mass: (a) X (nT) and (b) Y (nT).

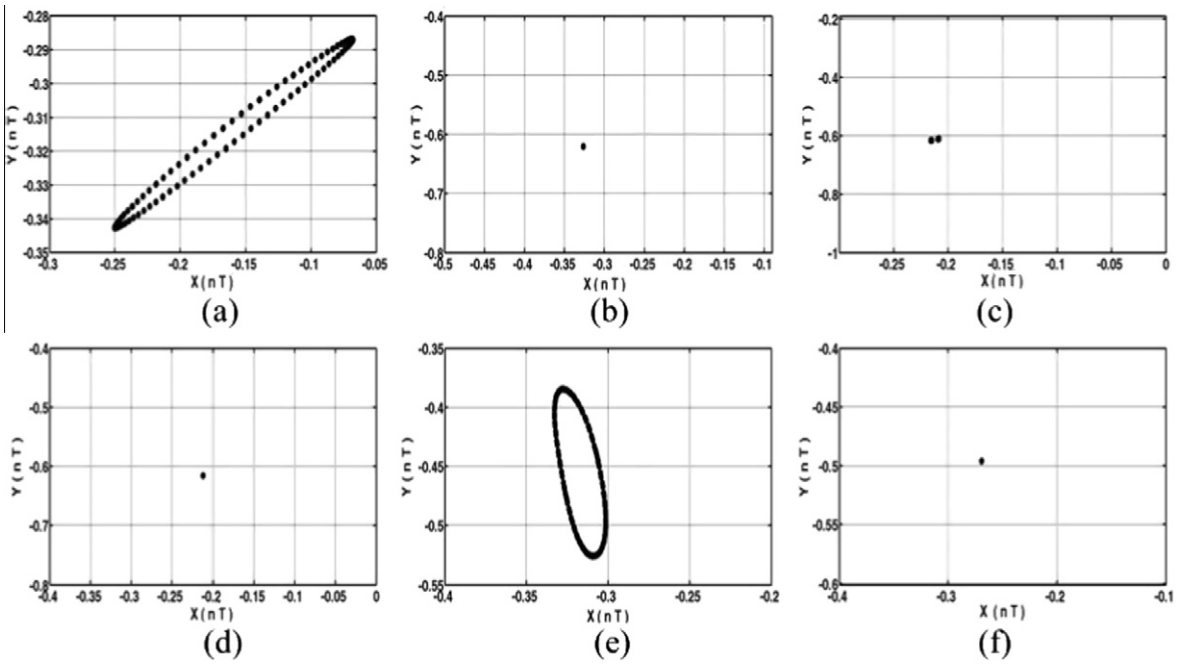

Fig. 7. Poincaré maps of rotor center trajectories at m_r = 1.1, 1.3, 1.9, 1.93, 3.16 and 3.46 kg.

Table 2
Variation of rotor center response with rotor mass over interval $1.0 \leqslant m_r \leqslant 4.0$ kg.

Rotor mass	[1.0, 1.25)	[1.25, 1.9)	[1.9, 1.93)	[1.93, 3.16)	[3.16, 3.46)	[3.46, 4.0]
Dynamic behavior	Quasi	T	$2T$	T	Quasi	T

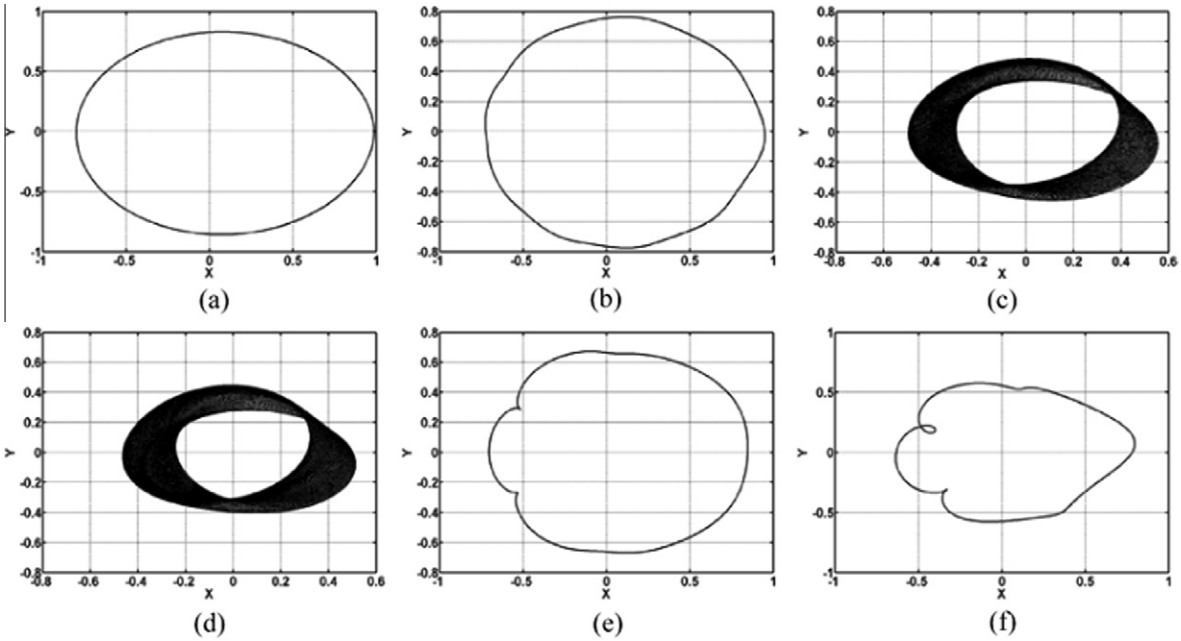

Fig. 8. Dynamic orbits of rotor center at $\Lambda_t = 1.2$, 2.4, 2.42, 3.21, 3.58 and 4.3.

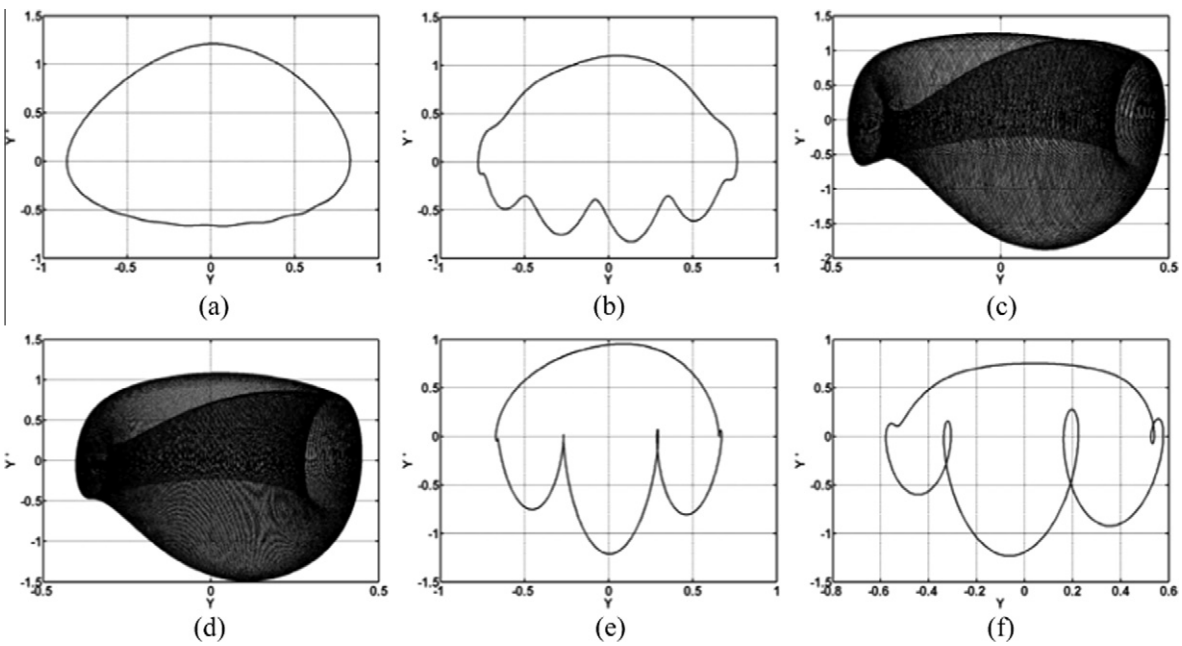

Fig. 9. Phase trajectories of rotor center at $\Lambda_t = 1.2$, 2.4, 2.42, 3.21, 3.58 and 4.3.

Note that in this study, the time-series data of the first 1000 revolutions are excluded from the dynamic behavior investigation so as to ensure that the analyzed data correspond to steady state conditions. The data include the orbital paths and velocity of the rotor center. These data are used to generate power spectra, Poincaré maps and bifurcation diagrams.

3. Results and discussions

3.1. Numerical analysis

Table 1 presents the Poincaré maps obtained by the SOR&FDM and DTM&FDM methods for the *T*-periodic orbits of the rotor center. It is observed that a good agreement by SOR&FDM and DTM&FDM exists between the two sets of results at different rotor mass and bearing number values for time step $\widetilde{H} = 0.01$. It also compares with different values of the time step, $\widetilde{H}$, for different rotor mass and bearing number values. It can be seen that the numerical results for time steps $\widetilde{H} = 0.001$ obtained by DTM&FDM are more precisely and even accurately to approximately four decimal places than those by SOR&FDM method. So, the DTM&FDM proposed in Section 2 are suitable for calculating the following results of rotor center and will obtain accurate data.

3.2. Dynamic analysis

The current dynamic analysis is considered two different situations: (1) the bearing number is maintained as a constant and the effect of increasing the rotor mass is examined and (2) the rotor mass is maintained as a constant and the effect of increasing the bearing number is investigated.

3.2.1. Situation 1

The gas journal bearing is loaded with a constant bearing number of $\Lambda_t = 1.27$ and the rotor mass m_r is specified as the bifurcation parameter.

3.2.1.1. Dynamic orbits and phase trajectories. Fig. 2 shows that the orbits of the rotor center are irregular at low values of the rotor mass ($m_r = 1.1$ kg), but become regular at rotor mass values of $m_r = 1.3$, 1.9, and 1.93 kg. For rotor mass value of $m_r = 3.16$ kg, the orbits exhibit non-symmetric and non-periodic motion. Finally, the rotor becomes regular at rotor mass values of $m_r = 3.46$ kg.

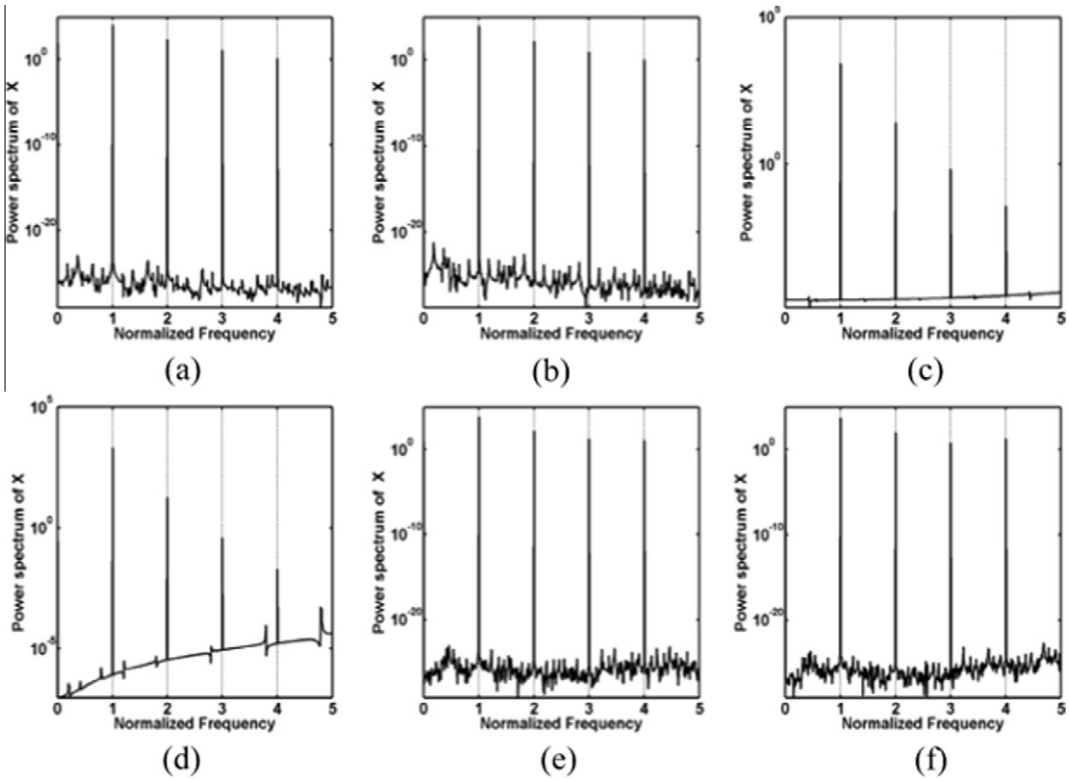

Fig. 10. Power spectra of rotor displacement in horizontal direction at $\Lambda_t = 1.2$, 2.4, 2.42, 3.21, 3.58 and 4.3.

Fig. 3 shows the phase trajectories of the rotor center at different values of the rotor mass. It is observed that the phase trajectories are regular at m_r = 1.3, 1.9, 1.93 and 3.46 kg, but become non-symmetric and irregular at rotor mass values of m_r = 1.1 and 3.16 kg.

3.2.1.2. Power spectra. Figs. 4 and 5 show the dynamic responses of the rotor center in the vertical and horizontal directions. It is seen that the rotor center exhibits quasi-periodic motion at rotor mass values of m_r = 1.1 kg. However, as the rotor mass is increased to m_r = 1.3, 1.93 and 3.46 kg, the power spectra (Figs. 4(b), (d), (f) and 5(b), (d), (f)) show that the orbits of the rotor center in the horizontal and vertical directions become periodic motion. For rotor mass value of m_r = 1.9 kg, the orbits exhibit sub-harmonic motion with a period of 2*T*. Finally, at rotor mass value of m_r = 3.16 kg, the orbits of the rotor center perform quasi-periodic motion in the horizontal and vertical directions.

3.2.1.3. Bifurcation diagrams. A bifurcation diagram summarizes the essential dynamics of a HSSAB system, and is therefore a useful tool for observing nonlinear dynamic behavior. The bifurcation diagrams presented in Fig. 6 plot the rotor center displacement against the rotor mass m_r. Qualitatively different behavior is observed at different values of m_r within the range 1.0–4.0 kg. Fig. 7(a)–(f) presents the Poincaré maps at m_r = 1.1, 1.3, 1.9, 1.93, 3.16 and 3.46 kg, respectively. Figs. 6(a), (b) and 7(a) show that the dynamic motion of the rotor center is quasi-periodic in both the *x*- and *y*-directions at lower values of the rotor mass, i.e. m_r < 1.25 kg. However, the quasi-periodic motion loses its stability at m_r = 1.25 kg and is replaced by periodic motion proof and shown in Fig. 7(b). As the mass is increased to m_r = 1.9 kg, the *T*-periodic motion is replaced by a 2*T*-periodic motion in the *x*- and *y*-directions shown in Fig. 7(c). Fig. 6 shows that this 2*T*-periodic motion is maintained over the interval $1.9 \leqslant m_r < 1.93$ kg. The 2*T*-periodic motion changes its motion at a rotor mass of 1.93 kg and is replaced by a *T*-periodic motion as shown in Fig. 7(d). Then, *T*-periodic motion is transferred to quasi-periodic motion at m_r = 3.16 kg (Fig. 7(e)). Finally, the rotor center changes its behavior as the rotor mass is increased to m_r = 3.46 kg and transits to *T*-periodic motion. It can be seen that there is a discrete point in the Poincaré map at m_r = 1.3, 1.93 and 3.46 kg, two discrete points at m_r = 1.93 kg and a closed curve at m_r = 1.1 and 3.16 kg. From the discussions above, it is evident that the behavior of the rotor center is dependent on the rotor mass. Table 2 summarizes the motions performed by the rotor center for rotor mass values in the range $1.0 \leqslant m_r \leqslant 4.0$ kg.

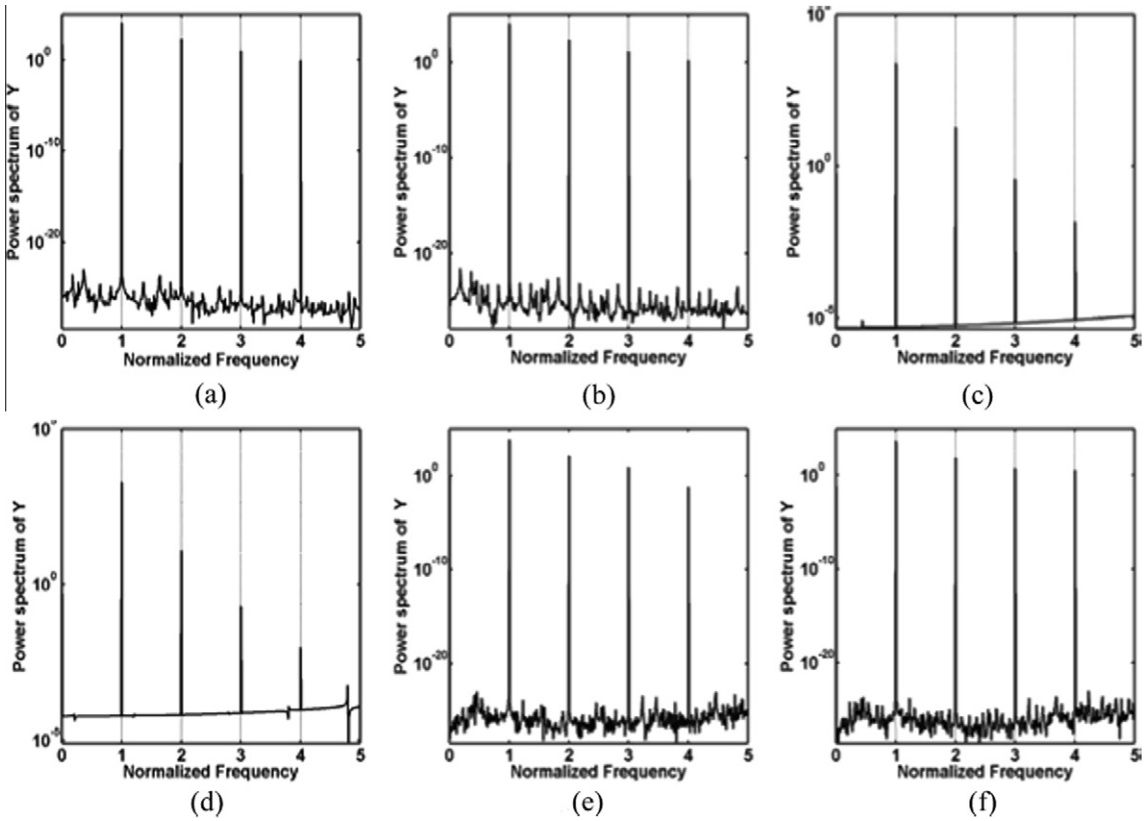

Fig. 11. Power spectra of rotor displacement in vertical direction at Λ_t = 1.2, 2.4, 2.42, 3.21, 3.58 and 4.3.

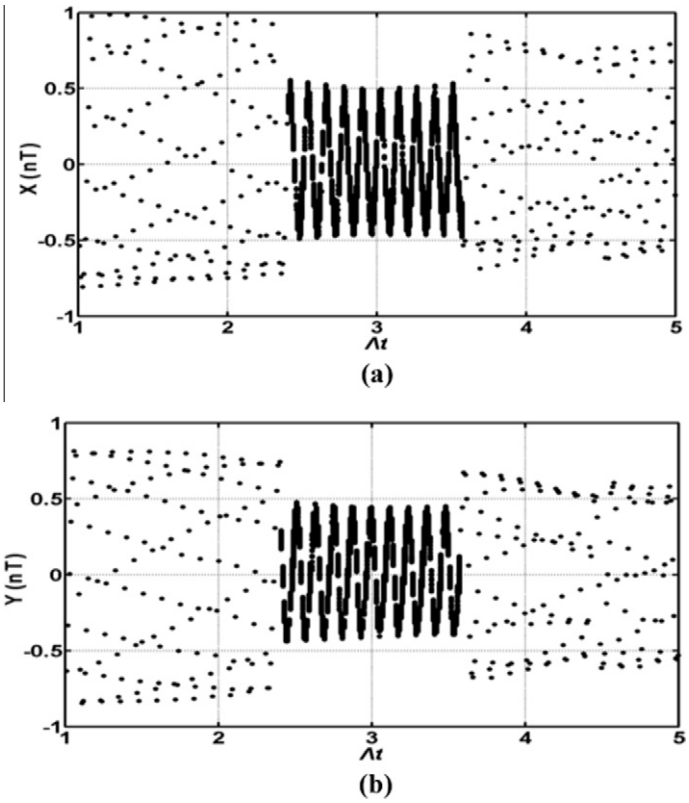

Fig. 12. Bifurcation diagrams versus bearing number: (a) X (nT) and (b) Y (nT).

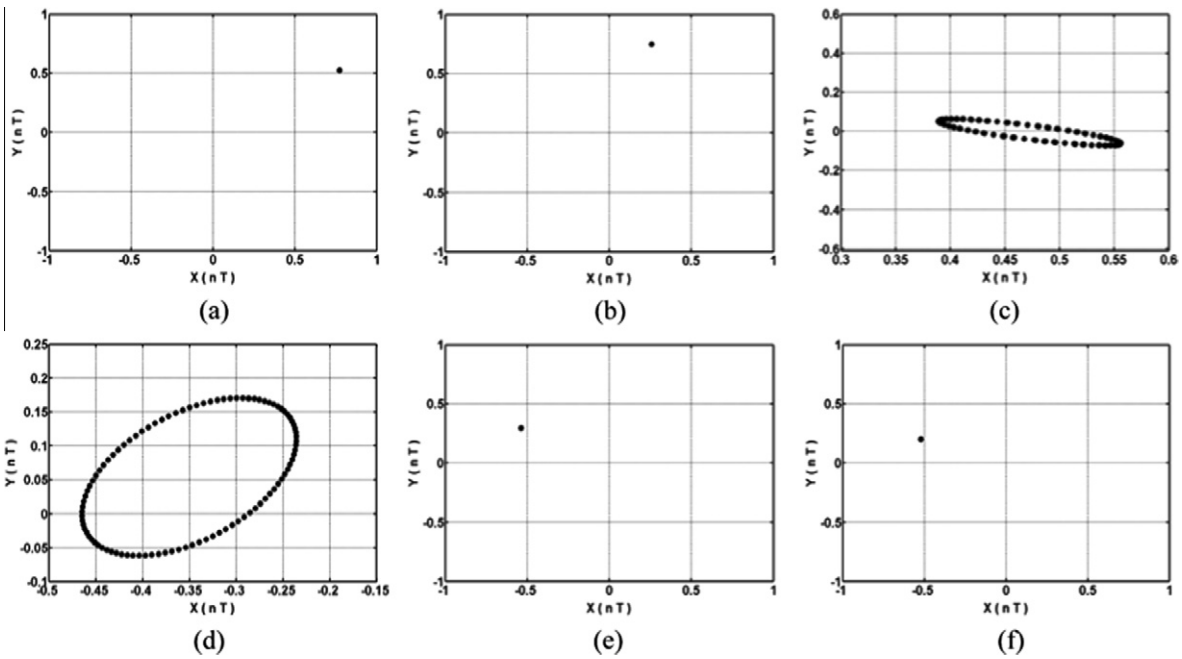

Fig. 13. Poincaré maps of rotor center trajectories at $\Lambda_t = 1.2$, 2.4, 2.42, 3.21, 3.58 and 4.3.

Table 3
Variation of rotor center response with bearing number over interval $1.0 \leqslant \Lambda_t \leqslant 5.0$.

Bearing number	[1.0,2.42)	[2.42,3.58)	[3.58,5]
Dynamic behavior	*T*	Quasi	*T*

3.2.2. Situation 2

The gas journal bearing is loaded with a constant rotor mass of $m_r = 2.5$ kg and the bearing number Λ_t is specified as the bifurcation parameter.

3.2.2.1. Dynamic orbits and phase trajectories. Fig. 8 shows that the orbits of the rotor center are regular and symmetry at low values of the bearing number (Λ_t=1.2 and 2.4), but become irregular at bearing number values of Λ_t=2.42 and 3.21. For bearing number value of $\Lambda_t = 3.58$ and 4.3, the orbits exhibit symmetric and periodic motion.

Fig. 9 shows the phase trajectories of the rotor center at different values of the bearing number. It is observed that the phase trajectories are regular at $\Lambda_t = 1.2$, 2.4, 3.58 and 4.3, but become non-symmetric and irregular at rotor bearing number of $\Lambda_t = 2.42$ and 3.21.

3.2.2.2. Power spectra. Figs. 10 and 11 show the dynamic responses of the rotor center in the vertical and horizontal directions. It is seen that the rotor center exhibits periodic motion at bearing number values of $\Lambda_t = 1.2$ and 2.4. However, as the bearing number is increased to $\Lambda_t = 2.42$ and 3.21, the power spectra (Figs. 10(c), (d) and 11(c), (d)) show that the orbits of the rotor center in the horizontal and vertical directions become quasi-periodic motion. Finally, at bearing number values of $\Lambda_t = 3.58$ and 4.3, the orbits of the rotor center perform periodic motion in the horizontal and vertical directions.

3.2.2.3. Bifurcation diagrams. The bifurcation diagrams presented in Fig. 12 plot the rotor center displacement against the bearing number Λ_t. Qualitatively different behavior is observed at different values of Λ_t within the range 1.0–5.0. Fig. 13(a)–(f) presents the Poincaré maps at $\Lambda_t = 1.2$, 2.4, 2.42, 3.21, 3.58 and 4.3, respectively. Figs. 12(a), (b) and 13(a), (b) show that the dynamic motion of the rotor center is *T*-periodic in both the *x*- and *y*-directions at lower values of the bearing number, i.e. $\Lambda_t < 2.42$. However, the *T*-periodic motion loses its stability at $\Lambda_t = 2.42$ and is replaced by quasi-periodic motion proof and shown in Fig. 13(c). Figs. 12 and 13(d) show that this quasi-periodic motion is maintained over the interval $2.42 \leqslant \Lambda_t < 3.58$. The quasi-periodic motion changes its motion at a bearing number of 3.58 and is replaced by a *T*-periodic motion as shown in Fig. 13(e). Finally, the rotor center persists *T*-periodic motion over the interval $3.58 \leqslant \Lambda_t \leqslant 5$. It can be seen that there is a discrete point in the Poincaré map at $\Lambda_t = 1.2$, 2.4, 3.58 and 4.3 and a closed curve at $\Lambda_t = 2.42$ and 3.21. From the discussions above, it is evident that the behavior of the rotor center is also dependent on the bearing number. Table 3 summarizes the motions performed by the rotor center for bearing number values in the range $1.0 \leqslant \Lambda_t \leqslant 5.0$.

4. Conclusions

This study has analyzed the influence of rotor mass and bearing number to a HSSAB system via a hybrid numerical method and presented the nonlinear behavior of a HSSAB system. Two different hybrid numerical methods included SOR&FDM and DTM&FDM are applied and compared to solve this system. The results show that DTM&FDM is more suitable for calculating the HSSAB system than SOR&FDM. So, the system state trajectories, power spectra, bifurcation diagrams, and Poincaré maps are solved by DTM&FDM and have revealed the presence of a complex dynamic behavior comprising periodic, sub-harmonic, and quasi-periodic responses of the rotor center. The results of this study provide an understanding of the nonlinear dynamic behavior of HSSAB systems with different rotor masses m_r and bearing numbers Λ_t.

Specifically, the results have shown that the rotor center behaves quasi-periodic motion over two intervals $1.0 \leqslant m_r < 1.25$ kg and $3.16 \leqslant m_r < 3.46$ kg. According to these two intervals, a heavier or lighter rotor will cause irregular and nonlinear motion. Periodic and sub-harmonic motions appear over $1.25 \leqslant m_r < 3.16$ kg and $3.46 \leqslant m_r < 4.0$ kg and behave regular and symmetry motions. Regarding the influence of the bearing number on the dynamic response of the bearing system, at $\Lambda_t = 1.2$ and 4.3, both of the Poincaré maps contain a single discrete point. However, as the bearing number is operated over the interval $2.42 \leqslant \Lambda_t < 3.58$, the *T*-periodic motion of the rotor center is replaced by quasi-periodic motion. Bearing number is relative to the rotational speed of rotor, so when design a HSSAB system, the bearing number is needed to be considered to avoid the nonlinear behavior appear.

Acknowledgment

The financial support of this research by National Science Council of ROC, under the Project No. NSC-97-2221-E-269-022 is greatly appreciated.

References

[1] J.S. Ausman, Linearized ph stability theory for translatory half-speed whirl of long self-acting gas-lubricated journal bearings, ASME J. Basic Eng. 3 (1963) 611–619.
[2] M. Botman, Experiments on oil film dampers for turbomachinery, ASME J. Eng. Power 98 (1976) 393–400.
[3] J.I. Nikolajsen, R. Holmes, Investigation of squeeze-film isolators for the vibration control of a flexible rotor, ASME J. Mech. Sci. 21 (1979) 247–252.
[4] X.H. Li, D.L. Taylor, Nonsynchronous motion of squeeze-film damper systems, ASME J. Tribol. 109 (1987) 169–176.
[5] F.F. Ehrich, High order subharmonic response of high speed rotor in bearing clearance, ASME J. Vib. Acoust. Stress Reliab. Design 110 (1988) 9–16.
[6] L.R. Gero, C.M.Mc.C. Ettles, An evaluation of finite difference and finite element methods for the solution of the Reynolds equation, ASLE Trans. 29 (2) (1985) 166–172.
[7] M. Malik, C.W. Bert, Differential quadrature solution for steady state incompressible and compressible lubrication problems, Trans. ASME, J. Tribol. 116 (1994) 296–302.
[8] C.C. Wang, M.J. Jang, Y.L. Yeh, Bifurcation and nonlinear dynamic analysis of a flexible rotor supported by relative short gas journal bearings, Chaos Soliton Fract. 32 (2007) 566–582.
[9] C.C. Wang, H.T. Yau, M.J. Jang, Y.L. Yeh, Theoretical analysis of the non-linear behavior of a flexible rotor supported by herringbone grooved gas journal bearings, Tribol. Int. 40 (2007) 533–541.
[10] C.C. Wang, H.T. Yau, Application of a hybrid numerical method to the bifurcation analysis of a rigid rotor supported by a spherical gas journal bearing system, Nonlinear Dynam. 51 (2008) 515–528.
[11] C.C. Wang, Application of a hybrid method to the nonlinear dynamic analysis of a spherical gas journal bearing system, Nonlinear Anal. – Theory Methods Appl. 70 (2009) 2035–2053.